Improved Lake Level Estimation From Radar Altimeter Using an Automatic Multiscale-Based Peak Detection Retracker

Jiaming Chen, Jingjuan Liao, and Chao Wang

***Abstract*—Satellite radar altimetry is an important technique for monitoring the water levels of oceans and inland water bodies, especially in areas where *in-situ* data are sparse or nonexistent. This study presented an automatic multiscale-based peak detection retracker (AMPDR). The retracker can extract a robust threshold level for each track, then the stable lake level can be obtained from the multipeak waveforms using a shortest-path algorithm. Additionally, the retracker can be used for mountain lakes and for flat lakes, and is also suitable for many kinds of altimetry data, such as those of Cryosat-2, Sentinel-3, and Jason-2/3. To validate the lake levels derived by the AMPDR retracker, the *in-situ* gauge data of seven lakes in the Tibetan Plateau and two lakes in a flat area are used. Moreover, seven existing retrackers are compared to evaluate the performance of the proposed AMPDR retracker. The results suggest that AMPDR can efficiently process many complex multipeak waveforms, and the AMPDR has the lowest mean of all track standard deviations over all lakes. The root-mean-squared error (RMSE) of the lake level time series obtained using AMPDR is the lowest over several lakes: The mean RMSEs of all the lakes overpassed by Cryosat-2, Sentinel-3, and Jason-2/3 are 0.149, 0.139, and 0.181 m, respectively. The AMPDR retracker is easy to implement, computationally efficient, and can give a height estimate for even the most contaminated waveforms.**

***Index Terms*—Lake level, multiscale-based subwaveform, retracker, satellite altimetry.**

I. Introduction

SATELLITE altimetry technology has been widely used since the 1990s to monitor water levels over inland waters [1]–[5]. This is because hydrological stations cannot be easily set up or the *in-situ* gauge data cannot be used publicly due to the limitations of the location and installation and maintenance costs [6], [7]. Therefore, satellite radar altimetry has been used to monitor the lake water level and storage variations at regional scales [2], [5], [8]–[10], to assess river dynamics, and estimate river floodplain discharge [11]–[13], and to calibrate hydrologic or hydrodynamic model parameters [14]–[17]. Compared with a traditional altimeter, a radar altimeter such as Sentinel-3 or Jason-2/3 displays a great improvement in the observation of nadir points. It operates with an open-loop tracking mode, which can control the return echo acquisition phase by properly setting its range window in time, based on prior on-board surface elevation information [18], [19]. Using synthetic aperture radar (SAR) technology, Cryosat-2, and Sentinel-3 can monitor inland water at a finer along-track resolution, and with interferometric SAR technologies, Cryosat-2 can determine the cross-track angle of arrival of the radar echoes [19], [20]. Although the data produced using these techniques improve the quality of observation points to some extent, there is still a problem of complex waveform pollution [4], [8], [21].

The quality of the water level data obtained from satellite altimetry can be improved by waveform retracking [1], that is, modifying the initial distance retrieved from the two-way travel time of radar short pulses sent to and reflected by the inland water surface. Many studies are available on the waveform retracking. Jain *et al.* [21] proposed a narrow primary peak retracker (NPPR) algorithm based on the maximum reflection power of the water surface to search the main peak of the echo with Cryosat-2 data. The algorithm can adjust the threshold according to the need, so it has strong adaptability. Villadsen *et al.* [8] developed a multiple waveform persistent peak (MWaPP) algorithm by assuming that one peak reflected by the inland water occurs in all waveforms, but other peaks reflected by other bright targets or off-nadir water bodies are less likely to be persistent, which could deal effectively with complex multipeak waveforms affected by land. Xue *et al.* [4] focused on Cryosat-2 synthetic aperture radar interferometer (SARin) waveforms and developed an improved ImpMWaPP retracker using a robust statistical method to obtain a reference water level and identifying the water-surface signal of the waveform based on this reference water level, thereby improving the processing performance for multipeak waveforms. Huang *et al.* [22] used an improved waveform retracking, called the TIC (50% Threshold and Ice-1 Combined algorithm) to derive water

Manuscript received July 6, 2020; revised September 27, 2020 and October 21, 2020; accepted October 31, 2020. Date of publication November 3, 2020; date of current version January 6, 2021. This work was supported in part by the National Natural Science Foundation of China under Grant 41871256 and in part by the Special Project for Talent Team Construction by the Henan Academy of Sciences under Grant 200501007. *(Corresponding author: Jingjuan Liao.)*

Jiaming Chen is with the Key Laboratory of Digital Earth Science, Chinese Academy of Sciences Aerospace Information Research Institute, Beijing 100094, China, and also with the Aerospace Information Research Institution, Chinese Academy of Sciences, Beijing 100094, China (e-mail: chenjiaming@aircas.ac.cn).

Jingjuan Liao is with the Key Laboratory of Digital Earth Science, Chinese Academy of Sciences Aerospace Information Research Institute, Beijing 100094, China, and also with the Key Laboratory of Earth Observation, Hainan Sanya 572029, China (e-mail: liaojj@aircas.ac.cn).

Chao Wang is with the Insitute of Geographical Sciences, Henan Academy of Sciences, Henan 450052, China (e-mail: 1208483461@qq.com).

Digital Object Identifier 10.1109/JSTARS.2020.3035686

levels in high-mountain regions with a complex terrain. Yuan *et al.* [23] proposed a novel multisubwaveform multiweight threshold retracker (MSMWTR) method for processing Jason-2 multipeak waveforms over medium-width rivers under rough and heterogeneous surfaces. Shu *et al.* [24] developed a new bimodal correction algorithm that could retrieve ice thickness and reliably estimate water levels for the ice-covered lakes in winter. However, the retrackers mentioned above could show poor performance in dealing with some complex multipeak waveforms affected by the rough terrain with steep changes and off-nadir observations, such as the waveforms available on Tibetan Plateau lakes [4]. Though these complex multipeak waveforms can be rejected by waveform classification in most cases, this is not desirable for small- and medium-sized lakes, which may result in serious data loss problems [25].

Since using a single radar altimeter to monitor the lake water level is often limited by temporal and spatial coverage, many researchers have used multialtimeter data to monitor lake water levels [2], [5], [9]. Nevertheless, there are problems with choosing different retracking algorithms for different altimeter data in the process of the monitoring lake water level using multialtimeter data. As there are different choices available, the accuracy of the water level data may be affected to some extent by the systematic bias among different retracking algorithms.

Therefore, this article considers the influence of off-nadir observations and rough terrain on waveforms, using a general statistical method to identify the leading edge of the waveform of the water-surface signal. This can improve the processing ability of the multipeak waveforms and can also be used for many different altimeter data. Furthermore, the proposed method is not limited by the surrounding area topography and, thus, can be used for mountain lakes and for flat lakes, which is of great significance in monitoring lake water level changes at large spatial scales. This article is organized as follows. First, we introduce the altimetry data and *in-situ* data used for validating our method, as well as our study areas in Section II. We describe the automatic multiscale-based peak detection retracker (AMPDR) algorithm methodology in detail in Section III. The results of the time series water level and of the track standard deviations from different retrackers are explained in Section IV. Section V gives the discussion and Section VI concludes this article.

II. Study Area and Data Used

A. Study Area

To ensure the representativeness and reliability of the results, seven lakes in the mountainous areas of the Tibetan Plateau were chosen as the study areas, and two lakes from floodplains in the lower reaches of rivers were chosen to compare with the mountain lakes. Each lake had *in-situ* water levels data and different characteristics (e.g., area, morphology, elevation, and surrounding landscape) (see Fig. 1). The seven mountain lakes were Qinghai Lake, Ngoring Lake, Bamco, Nam Co, Zhari Namco, Dagze Co, and Dawa Co, and the two floodplain lakes were Dongping Lake and Taihu Lake. They had the following characteristics.

1) The surrounding topography features large fluctuations, with the maximum change being up to several hundred meters in altitude.
2) Qinghai Lake and Ngoring Lake, located in the northeast of the Tibetan Plateau, are in the Qaidam Basin and Yellow River Basin, respectively. The other lakes in the Tibetan Plateau are in the Qiangtang Basin.
3) Dongping Lake and Taihu Lake are located in the Yellow River Basin and Yangtze River Basin, respectively. The precipitation is abundant, and torrential rain floods occur [26].
4) All the lakes located in the Tibetan Plateau have rarely been affected by human activities.
5) Dongping Lake is an artificial lake with water levels controlled by a management agency.
6) Ice formations on these lakes are present in winter, except for Taihu Lake. The freezing time is generally from November of one year to April of the following year [4].

B. Data Used

Three datasets were used in this study: Cryosat-2, Sentinel-3, and Jason-2/3 missions. SIRAL, carried by Cryosat-2, obtains elevation information using the SARin in the Tibetan plateau and allows the across track angle offset of the echoing point to be determined directly; thus, off-nadir correction can be removed effectively [20]. Jason-2/3 and Sentinel-3 data operate with an open-loop tracking mode, which can improve observation efficiency and obtain good quality data in some areas such as in the lake coastal regions or in narrow channels. This mode offers enhanced capabilities with respect to the closed-loop tracking mode over the areas mentioned above [18], [19]. This makes it possible to monitor water levels changes in small lakes. The Cryosat-2, Sentinel-3, and Jason-2/3 data are selected in this article to verify the applicability of the retracking algorithm to multialtimeter data.

The *in-situ* data of the nine lakes were selected in this study, and Table I lists the measurement time and other information. The *in-situ* data for Ngoring Lake and Qinghai Lake were from the Hydrology and Water Resources Survey Bureau in Qinghai Province. While the *in-situ* data for Dongping Lake and Taihu Lake were from the Yellow River Commission of the Ministry of Water Resources[1] and the Department of Water Resources of Jiangsu Province, respectively. Additionally, the *in-situ* data from the Institute of Tibetan Plateau Research, Chinese Academy of Sciences[2] were available on Nam Co, Zhari Namco, Bamco, Dagze Co, and Dawa Co.

III. Methodology

A. Lake Water Level Estimation

For extracting satellite altimetry, it is necessary that water levels need to select correct ground tracks and valid footprints falling on the lakes. This problem can be addressed by comparing

[1] [Online]. Available: http://www.yellowriver.gov.cn/
[2] [Online]. Available: http://www.tpedatabase.cn/

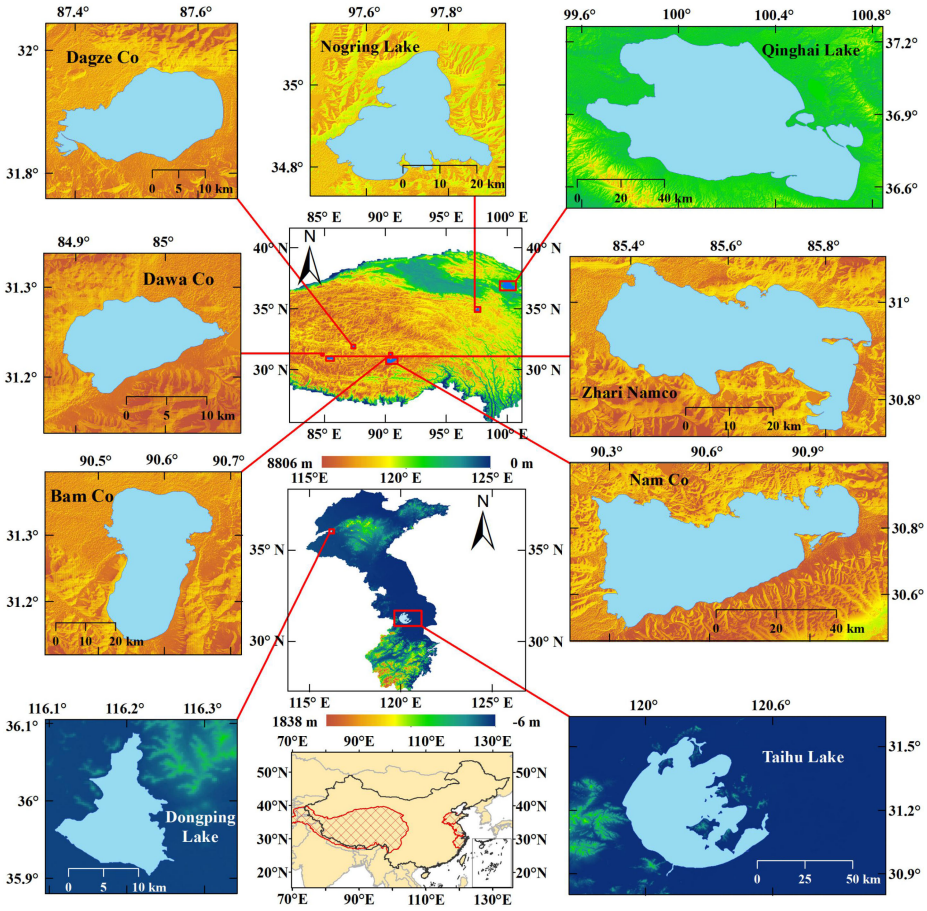

Fig. 1. Geographical locations and shape of the study area.

the geographic coordinates of the footprints with the lake-shape dataset. After picking out the valid footprints, the lake surface height can be calculated for each footprint:

$$H = \mathrm{Alt} - (R_{\mathrm{range}} + \Delta R_{\mathrm{dry}} + \Delta R_{\mathrm{wet}} + \Delta R_{\mathrm{iono}} + \Delta R_{\mathrm{tide}} + \Delta R_{\mathrm{retrack}}) - N_{\mathrm{geoid}} \quad (1)$$

where Alt is the satellite altitude, R_{range} is the distance between the altimeter and lake surface, ΔR_{dry} is the dry troposphere, ΔR_{wet} is the wet troposphere, ΔR_{iono} is the ionosphere correction, ΔR_{tide} includes the solid earth tide, pole tide, and ocean tide correction, and $\Delta R_{\mathrm{retrack}}$ is the retracking correction. N_{geoid} is the geoid height with respect to the ellipsoid; the 2008 Earth Gravitational Model [27] was used in this article. Except for $\Delta \mathrm{R}_{\mathrm{retrack}}$, all the corrections mentioned above were included in the altimetry data product.

Additionally, to validate the water levels derived from the different algorithms, two steps were required for processing. 1) After removing the abnormal track point levels by visual inspection, the lake level time series was obtained using the "R" package tsHydro[3]. The core of tsHydro is a state space [28], which consists of a process model and an observation model. 2) The track mean level was obtained from the lake level time series calculated above, then the track standard deviation of the lake level was obtained after removing the outliers using one standard deviation from the track mean level.

[3][Online]. Available: https://github.com/cavios/tshydro

B. Automatic Multiscale-Based Peak Detection Retracker

A new AMPDR algorithm was developed for this study. The algorithm assumed that each passing observation except invalid off-nadir points must have a leading edge of a waveform reflected by the water directly beneath the satellite. In addition, the leading edge may appear in the range of other local peaks under the influence of land signals, instead of as the primary peak described in [21], as shown in Fig. 2. Fig. 2(a) and (b) is the two waveforms near the shore with their location illustrated in Fig. 2(c). The red line was transformed by the *in-situ* data of April 16, 2016, for which the system bias was removed by calculating the difference between the track level time series and the *in-situ* level series. For Fig. 2(a), if the primary peak only is considered, a retracking error will occur. In fact, the reflected signal from the water surface appears at the third peak of the waveform according to the *in-situ* data, which may be caused off-nadir points. Fig. 2(b) illustrates a typical multipeak waveform, which may be caused by a land signal or other discrete bright targets [26], and the reflected signal from the water surface appears at the third peak of the waveform rather than at the

TABLE I
DETAILS OF THE *IN-SITU* DATA OF NINE LAKES VALIDATED

Lake Name	Date	Reference	Continuous	Mode
Qinghai Lake	01/2016-08/2019	1985[a]	No	Absolute
Nogring Lake	01/2010-12/2015	1985[a]	Yes	Absolute
Dongping Lake	04/2016-07/2019	1985[a]	No	Absolute
Taihu Lake	11/2017-09/2019	1985[a]	Yes	Absolute
Bamco	06/2013-10/2017	Customize	No	Relative
Zhari Namco	01/2016-10/2017	Customize	No	Relative
Nam Co	03/2010-12/2016	1985[a]	Yes	Absolute
Dagze Co	06/2013-10/2016	Customize	Yes	Relative
Dawa Co	06/2013-10/2016	Customize	Yes	Relative

[a]1985 stands for 1985 national elevation benchmarks in China.

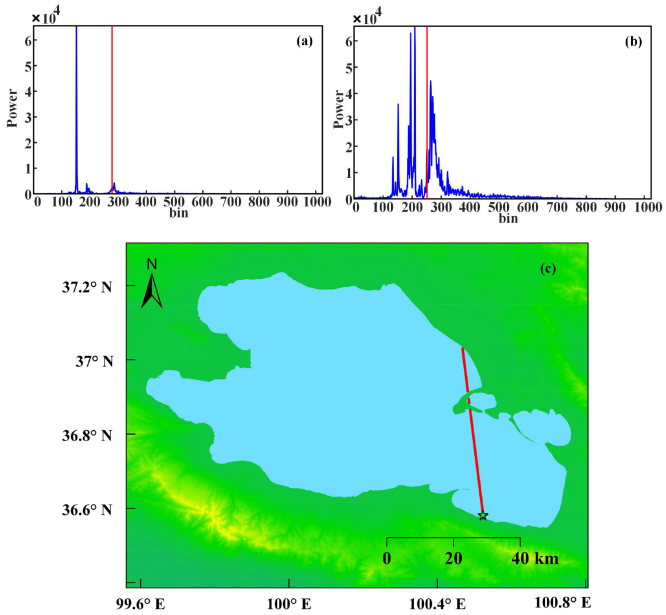

Fig. 2. Two waveform data from Cryosat-2 crossing Qinghai Lake on April 16, 2016 corresponding to highlighted (green) points in (c) (the red line is the location of water surface signal reflection based on *in-situ* data).

primary peak. This method simply tries to determine the bins in the waveform where the reflection from the water surface at nadir is most likely found. Accordingly, after detecting all the subwaveforms that may contain water surface reflection signals, the best subwaveform containing the water surface reflection signal could be determined using a statistical method. Since the range to the water body at nadir should be close in all waveforms, the observation contaminated by the land signal could also be used to obtain the accurate water level information.

The AMPDR algorithm includes the following steps:

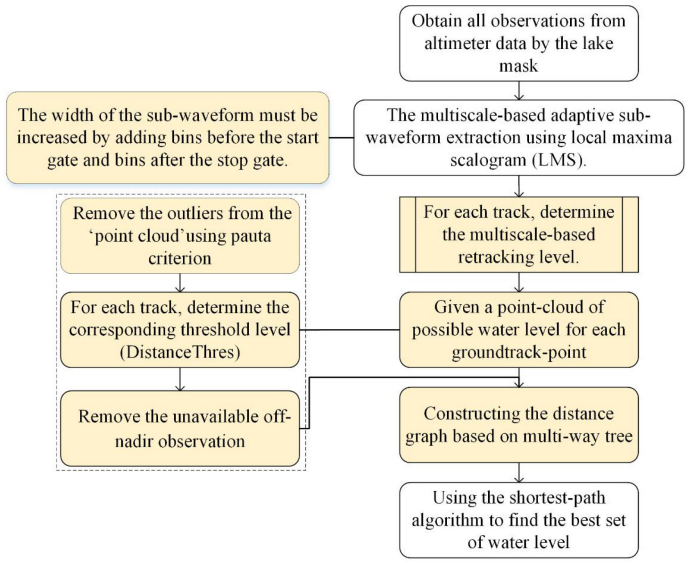

Fig. 3. Flowchart describing the AMPDR. Steps with yellow background are the preparation for using the shortest path algorithm.

1) automatic multiscale-based peak detection;
2) multiscale-based adaptive subwaveform extraction;
3) multiscale-based adaptive subwaveform retracking calculation;
4) selection of off-nadir that does not catch the water surface reflection signal;
5) final determination of the retracking level by applying a shortest-path algorithm.

The steps of the new retracker are illustrated in Fig. 3. To simplify the algorithm description, the start gate and the stop gate of the subwaveform window are described by *startgate* and *stopgate*, respectively.

1) Multiscale-Based Adaptive Subwaveform Extraction: In this article, a method based on the local maxima scalogram (LMS) [29] is used to detect the peak of the waveform, and its core function is to construct and analyze an $L \times N$ local maxima matrix $(m_{k,i})_{L\times N}$, which is a matrix comprising the scale-dependent occurrences of local maxima.

First, to calculate the LMS, the local maxima of the waveform are determined using a moving window approach whereby the window length w_k is varied $\{ w_k = 2k+1 | k = 1, 2, \ldots, L\}$. The local maxima value $m_{k,i}$ for the varied window length w_k can be determined according to

$$m_{k,i} = \begin{cases} 0, & x_{i-1} > x_{i-k-1} \cap x_{i-1} > x_{i+k-1} \\ r+1, & \text{otherwise} \end{cases} \tag{2}$$

where r is a uniformly distributed random number in the range [0, 1], k is the kth scale of the waveform, x is the power waveform, $L = 5$ is the best situation for peak detection in this study, For $i = 1, \ldots, k+1$, and for $i = N-k+2, \ldots, N$ the value $r+1$ is assigned to $m_{k,i}$, these operations of (2) result in the matrix $M = (m_{k,i})_{L\times N}$.

Second, a rowwise summation of the LMS matrix *M* is calculated

$$\gamma_k = \sum_{i=1}^{N} m_{k,i}\ ,\ k\ =\ 1, 2, \ldots, L. \tag{3}$$

The rowwise summation $\gamma\ =\ [\gamma_1, \gamma_2, \ldots, \gamma_L]$ contains information about the scale-dependent distribution of zeros (and, thus, local maxima), then the global minimum of γ, $\lambda\ =\ \mathrm{argmin}(\gamma_k)$, is obtained, representing the scale with the most local maxima. Additionally, the value λ is used to reshape the LMS matrix *M* by removing the elements $m_{k,i}$ for which $k > \lambda$ holds, leading to a new matrix $M_r = (m_{k,i})_{\lambda \times N}$.

Third, the peaks are detected by calculating the columnwise standard deviation of the matrix M_r according to (4). All indices i for which $\sigma_i = 0$ holds are the bins of the peak of the waveform that may contain the surface water reflection signal, which are assigned to the stopping point of subwaveform ($\mathrm{stopgate}_i$). For each waveform of the observation, we can get a vector $\mathrm{stopgate}\ =\ [\mathrm{stopgate}_1, \mathrm{stopgate}_2, \ldots, \mathrm{stopgate}_{\hat{N}}]$. It is notable that detected peaks are valid only if the corresponding power value is greater than $0.05 \times M_{\mathrm{thres}}$ because the AMPD algorithm will detect some peaks with very low power, which are usually caused by noise.

$$\sigma_i = \frac{1}{\lambda - 1}\left[\sum_{k\,=\,1}^{\lambda}\left(m_{k,i} - \frac{1}{\lambda}\sum_{k\,=\,1}^{\lambda} m_{k,i}\right)^2\right]^{\frac{1}{2}} \tag{4}$$

$$M_{\mathrm{thres}} = \frac{\sum x^4}{\sum x^2}. \tag{5}$$

Finally, to determine each starting gate of subwaveform ($\mathrm{startgate}_i$) corresponding to the $\mathrm{stopgate}_i$, several processing steps are required.

1) The waveform is normalized with the maximum power.
2) The power difference in consecutive bins is calculated.
3) Going backwards from each $\mathrm{stopgate}_i$, $\mathrm{startgate}_i$ is determined at the first gate in which the power difference in consecutive bins is lower than 0.001 units.

According to the method mentioned above, for each waveform of the observation we can get $\mathrm{startgate}\ =\ [\mathrm{startgate}_1, \mathrm{startgate}_2, \ldots, \mathrm{startgate}_{\hat{N}}]$, along with $\mathrm{stopgate}$ to form $\hat{N}$ subwaveforms for the observation. It was found that the subwaveform in some situations was only one to three bins wide. This narrow width of the subwaveform is inadequate to obtain the level. Thus, the width of the subwaveform must be increased by adding bins before the starting point and bins after the stopping point. It is found that the width of the subwaveform needs to be at least five bins (two bins after the stopping point and one or two bins before the starting point if necessary).

2) Multiscale-Based Adaptive Subwaveform Retracking Calculation: The subwaveform center of gravity (COG) retracker [21], [30] and subwaveform threshold retracker were used to calculate the $\hat{N}$ multiscale subwaveform retracking water level. The computation of the subwaveform COG retracker uses the parameters COG and *W*, and the retracking bin location $C_{\mathrm{retrack\_COG}}$ is calculated as in (6). The subwaveform threshold retracker is an extension to the subwaveform COG retracker and uses the parameter *M* computed in the subwaveform COG retracker. The purpose is to identify the first bin location ithres, where the power of the bin exceeds the Threshold. The threshold retracking bin location $C_{\mathrm{retrack\_Thres}}$ is calculated as in (7). In this article, all possible $\hat{N}$ subwaveforms for each waveform of the nadir point are needed to obtain the possible water level using the retracker.

$$C_{\mathrm{retrack\_COG}} = \mathrm{COG} - W/2 \tag{6}$$

$$C_{\mathrm{retrack\_Thres}} = \mathrm{ithres} - 1 + \frac{\mathrm{Threshold} - P_{\mathrm{ithres}-1}}{P_{\mathrm{ithres}} - P_{\mathrm{ithres}-1}}. \tag{7}$$

It should be noted that we set the Threshold as $0.5 \times M$ in the subwaveform threshold retracker. M is the amplitude of the subwaveform, W is the width of the subwaveform, and COG is the center of gravity of the subwaveform. In this article, the algorithm using a 50% threshold retracker is called AMPDTR, and the algorithm using the COG retracker is called AMPDOR.

3) Determination of the Retracking Level Using Shortest-Path Algorithm: According to the method mentioned above, we use all $\hat{N}$ subwaveforms for each waveform of the nadir point, which may contain the water surface reflection signal and can be used for retracking, for water level estimation. We end up with several equally likely water levels at each measurement location of the nadir point that could be thought to form a "point-cloud," a set of heights containing the possible water levels from the waveform of each nadir point for a track. Given now a "point-cloud" of a (equally) possible water level for each track point, we need to realize a consistent value of the water level at each measurement position by finding the optimal water level candidates. Consequently, the problem of finding the optimal retracking water level can be transformed into a shortest-path optimization problem of a "point-cloud" with certain constraints. Furthermore, before applying a shortest-path algorithm, the outliers, and the invalid off-nadir observation from the "point-cloud" need to be rejected, which can be detected by the following steps.

1) Remove the outliers from the "point-cloud" through the 3σ criterion (loop three times, which is efficient in the experiment, and does not delete too many elevation values).
2) Round the water level for each measurement location for each track, and construct the cumulative distribution function (CDF) of these rounded levels. After this, we can obtain the distance corresponding to the minimum second-order difference quotient of this CDF, which is considered as $\mathrm{DistanceThres}$. Fig. 4(a) shows the construction of CDF for the track over Qinghai Lake on April 16, 2016.
3) Calculate the difference between the average of the multiple-scale water level at each measurement location and the threshold $\mathrm{DistanceThres}$ given in step (b). The level from invalid off-nadir observation usually shows a large bias with the $\mathrm{DistanceThres}$. So, if the difference is larger than the half of the range window, it may not provide the signals from water surface and this observation will be regarded as an invalid off-nadir point (using Sentinel-3 as an example, it is 1/2∗128∗0.4684).

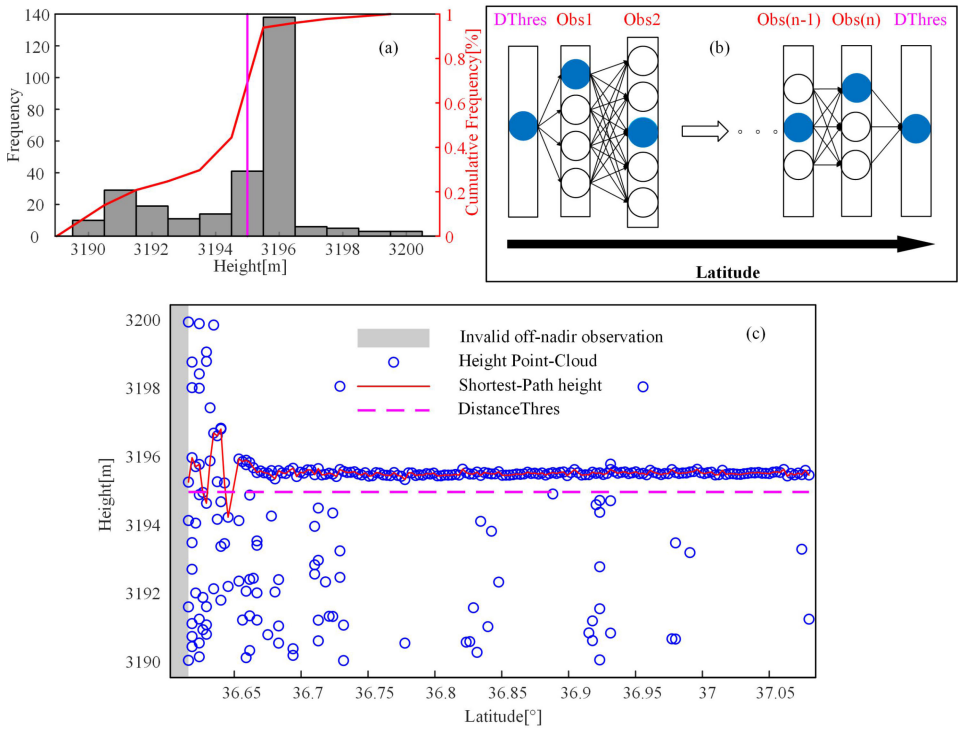

Fig. 4. (a) Histogram and the CDF from the track in (c). (b) Schematic illustration of optimal water level estimation employing Dijkstra algorithm. (c) Exemplary water level point cloud from Qinghai Lake on January 22, 2016.

After removing the obvious noise signals and the invalid off-nadir observations, the resulting set of the remaining levels is then used to construct the "point-cloud" and to estimate the optimal water level at each measurement location. We chose the Dijkstra algorithm [31] in this article, where a distance graph is constructed according to a multitree method, as shown in Fig. 4(b). Every water level value per observation point is assigned to one layer, and the layer is lined up according to the latitude, from low to high. In addition, for the start and end node of the Dijkstra distance graph, we use the value DistanceThres. Dijkstra's method requires the choice of edge weights between individual-connected nodes. In our application, we chose the height differences between connected nodes as edge weights. From Fig. 4(c), it can be seen that the waveforms with latitude less than 36.66 all show obvious multipeaks, which are mainly caused by contamination of the land signal. In particular, the waveforms with latitude less than 36.60 were detected as invalid off-nadir observation. Finally, the optimal water levels at each measurement location can also be found by finding the shortest path except for the invalid off-nadir observations.

IV. Results

A. Comparison of Retracking Methods

The performance of AMPDR was evaluated by comparing AMPDTR and AMPDOR to other algorithms. All the four altimeter data were processed using the following algorithms: NPPTR (Narrow Primary Peak Threshold retracker) with a 50% threshold level (NPPTR [0.5]) and with a 80% threshold level (NPPTR [0.8]) [21], NPPOR (Narrow Primary Peak OCOG Retracker) [21], and the MWaPP retracker [8]. In addition, according to the characteristics of the data, the ESA L2 retracker (Wingham/Wallis) [32] is used for Cryosat-2 data, the SAR Altimetry Mode Studies and Applications (SAMOSA) retracker [33] is used for Sentinel-3 data, and the ALES+ retracker [34] is used for Jason-2/3 data. The SAMOSA retracker height could be obtained from "range_ocean_20_ku" of Sentinel-3 L2 level data, and the ALES+ retracker height level was calculated by the method presented in Passaro *et al.* [34]. To compare the performance of the different retracking methods with different data, some examples of the results for some tracks crossing Nam Co, Dagze Co, and Zhari Namco are shown in Figs. 5, 6, and 7, respectively. Looking at the detailed plots in Figs. 5(c), 6(c), and 7(c), it can be seen that different algorithms have different abilities to deal with different waveforms, but the results from AMPDR are less noisy for the different altimeter data, especially in some measurement locations close to the shore. Therefore, AMPDR appears to provide the best and the most robust results. Furthermore, all the retrackers except for AMPDR have a problem of losing the water level during processing of the multipeak waveform, such as the height retrieved around 30.67°N crossing the Nam Co and around 31.01°N crossing the Zhari Namco. This is mainly due to the removal of the abnormal retracking water level greater than 4730 m and lower than 4605 m to show the figures more clearly, respectively. Actually, the measurements close to the lakeshore are severely corrupted when CryoSat-2 flies from south to north. This is not only because the data are contaminated by land noise, but also because the weaker geoid residual may be hidden in the noisy water levels [35]. From Figs. 5(b), 6(b), and 7(b), it can be seen that the AMPDR algorithm obtains a result much closer to the *in-situ* data. It should be noted that the AMPDR algorithm can effectively avoid this kind

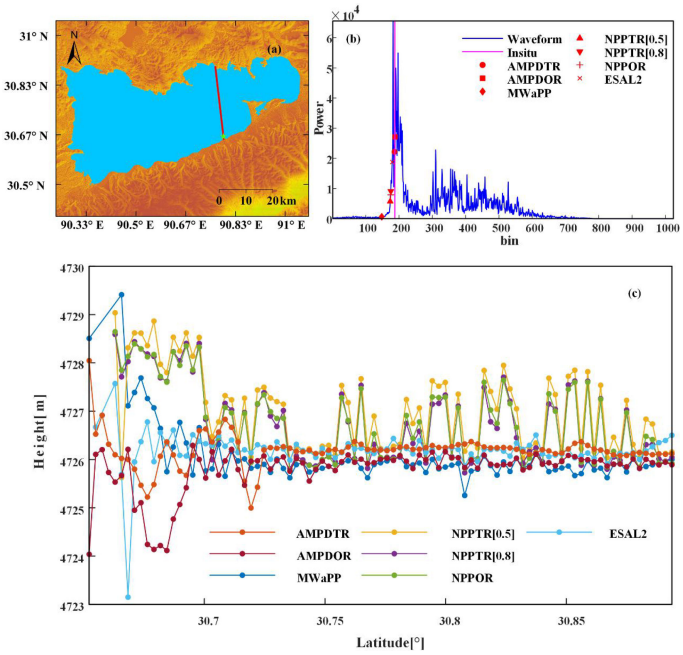

Fig. 5. (a) Track of Cryosat-2 cross over Nam Co on 20 July 2011. (b) Retracking results for different methods corresponding to highlighted (green) points in (a). (c) Spatial distribution of water level in Nam Co obtained by different retracking algorithms.

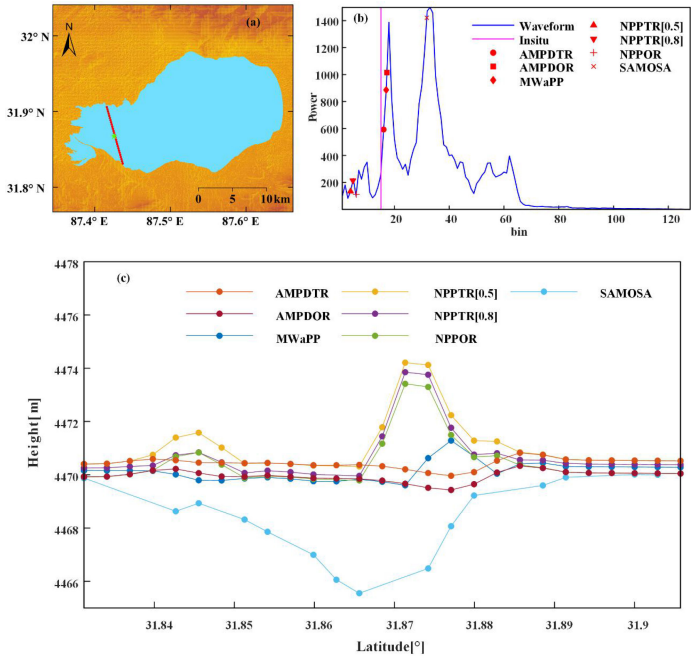

Fig. 6. (a) Track of Sentinel-3 cross over Dagze Co on 4 May 2016. (b) Retracking results for different methods corresponding to highlighted (green) points in (a). (c) Spatial distribution of water level in Dagze Co obtained by different retracking algorithms.

of noise interference when there is large noise in the leading edge of the water signal, while the performance of retracking methods such as MWaPP will be greatly affected. Consequently, the AMPDR algorithm can obtain a more stable retracking level, and can also successfully deal with more pollution observations, indicating that it may also have the potential to monitor the water levels of small- and medium-sized lakes or some rivers. In general, the AMPDR retracker provides better results than other retrackers during processing of the multipeak waveform.

B. Standard Deviations of Overpasses

The standard deviations are mostly affected by the location of the track with respect to the shore of the inland surface and the number of observation points within each along-track. Higher standard deviations are usually seen in data that are seriously affected by surrounding heterogeneous surfaces. Accordingly, the mean standard deviation of all the retracking water levels can be used to show the performance of different algorithms in processing different waveforms. Before calculating the standard deviations of all the retracking water levels, the differences between the retracking levels and the mean levels larger than 20 m were removed. The smaller the standard deviation, the better the retracking performance [8], [28]. Table II lists the means of all track standard deviations for each retracker over each lake. It can be seen that AMPDTR has the lowest results for Sentinel-3 and Jason-2/3 data, while AMPDOR has the lowest results for Cryosat-2 data. In fact, NPPTR [0.5], NPPTR [0.8], and NPPOR give similar results, but are worse than the other retrackers when processing the multipeak waveforms. Due to the topography around the inland surface, the reflected signal

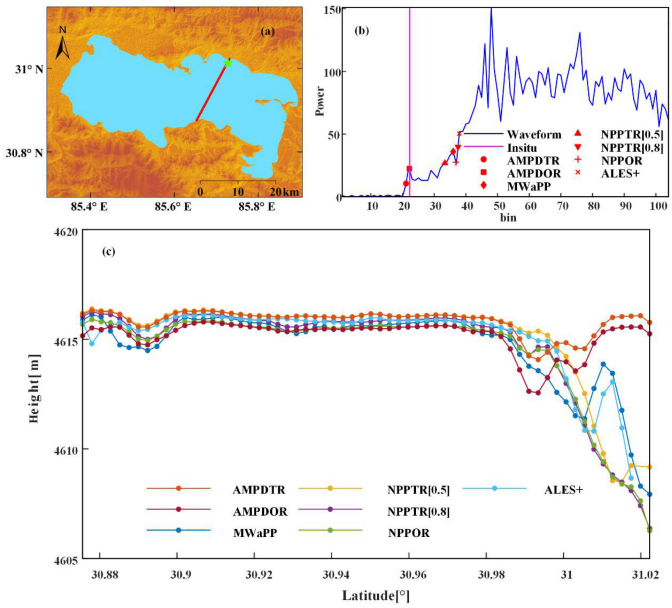

Fig. 7. (a) Track of Jason-2 cross over Zhari Namco on 30 October 2016. (b) Retracking results for different methods corresponding to highlighted (green) points in (a). (c) Spatial distribution of water level in Zhari Namco obtained by different retracking algorithms.

of the water surface from some observation points may not enter the range of the tracking window, resulting in multipeak waveforms. Consequently, the mean standard deviations of the water level obtained by the SAMOSA and ALES+ algorithms based on a theoretical waveform are above 0.4 m, while the

TABLE II
MEANS OF TRACK LEVEL STANDARD DEVIATIONS AND IMPROVE PROPORTION DERIVED[A] BY THE DIFFERENT RETRACKERS OVER THE NINE LAKES

	Lake Name	AMPDTR	AMPDOR	MWaPP	NPPTR [0.5]	NPPTR [0.8]	NPPOR	ESA L2	SAMOSA	ALES+
Cryosat-2	Ngoring Lake	0.154	0.154	0.139	0.268	0.254	0.255	0.156		
		[0.929]	[0.929]	[0.936]	[0.876]	[0.883]	[0.882]	[0.928]		
	Qinghai Lake	0.102	0.098	0.135	0.393	0.378	0.380	0.159		
		[0.954]	[0.956]	[0.939]	[0.823]	[0.830]	[0.829]	[0.928]		
	Nam Co	0.174	0.157	0.200	0.455	0.448	0.442	0.191		
		[0.943]	[0.948]	[0.934]	[0.850]	[0.852]	[0.854]	[0.937]		
	Zhari Namco	0.192	0.137	0.201	0.526	0.505	0.499	0.162		
		[0.936]	[0.954]	[0.933]	[0.825]	[0.832]	[0.834]	[0.946]		
	Bamco	0.126	0.116	0.199	0.639	0.609	0.624	0.164		
		[0.942]	[0.946]	[0.908]	[0.703]	[0.717]	[0.710]	[0.924]		
	Dagze Co	0.196	0.186	0.297	0.797	0.746	0.770	0.382		
		[0.921]	[0.925]	[0.880]	[0.679]	[0.699]	[0.689]	[0.846]		
	Dawa Co	0.171	0.155	0.628	0.763	0.757	0.753	0.532		
		[0.909]	[0.918]	[0.666]	[0.595]	[0.598]	[0.600]	[0.717]		
Sentinel-3	Dongping Lake	0.250	0.169	0.347	0.873	0.867	0.831		0.463	
		[0.276]	[0.509]	[-0.005]	[-1.530]	[-1.512]	[-1.407]		[-0.340]	
	Taihu Lake	0.217	0.438	0.660	1.227	1.232	1.230		0.838	
		[0.524]	[0.039]	[-0.448]	[-1.690]	[-1.701]	[-1.698]		[-0.837]	
	Qinghai Lake	0.114	0.106	0.165	0.198	0.201	0.193		0.239	
		[0.710]	[0.729]	[0.581]	[0.497]	[0.489]	[0.509]		[0.391]	
	Nam Co	0.100	0.126	0.144	0.165	0.176	0.154		0.139	
		[0.704]	[0.627]	[0.573]	[0.510]	[0.480]	[0.543]		[0.589]	
	Zhari Namco	0.159	0.163	0.210	0.174	0.184	0.179		0.236	
		[0.643]	[0.634]	[0.527]	[0.608]	[0.587]	[0.598]		[0.468]	
	Dagze Co	0.124	0.123	0.166	0.256	0.261	0.253		1.050	
		[0.586]	[0.590]	[0.447]	[0.147]	[0.131]	[0.158]		[-2.499]	
Jason2	Ngoring Lake	0.322	0.381	0.396	0.420	0.463	0.448			0.662
		[0.799]	[0.763]	[0.753]	[0.738]	[0.711]	[0.721]			[0.587]
	Qinghai Lake	0.206	0.227	0.242	0.217	0.234	0.216			0.378
		[0.890]	[0.880]	[0.871]	[0.885]	[0.876]	[0.885]			[0.799]
	Zhari Namco	0.157	0.211	0.262	0.172	0.209	0.186			0.427
		[0.825]	[0.765]	[0.708]	[0.809]	[0.768]	[0.793]			[0.525]
Jason3	Zhari Namco	0.264	0.317	0.410	0.314	0.354	0.328			0.368
		[-1.471]	[-1.977]	[-2.841]	[-1.946]	[-2.323]	[-2.074]			[-2.446]

[a]The Improve Proportion Derived are written in square brackets.

mean standard deviations of the level obtained by AMPDTR using Cryosat-2, Sentinel-3, and Jason-2/3 are 0.160, 0.161, and 0.237 m, respectively. This shows that the water levels derived by AMPDR are the most stable, and it has the potential to monitor the water levels of medium and small lakes using a radar altimeter. Moreover, the Improvement Percentages (IMP) can also be used to evaluate the performance of the retracking algorithms:

$$\mathrm{IMP} = \frac{\sigma_{\mathrm{unretracked}} - \sigma_{\mathrm{retracked}}}{\sigma_{\mathrm{unretracked}}} \tag{8}$$

where $\sigma_{\mathrm{unretracked}}$ is the mean of the standard deviation of the water level without retracking correction, and $\sigma_{\mathrm{retracked}}$ is the mean of the standard deviation of the retracking water level. A negative improvement percentage indicates that retracking deteriorates the water level. Table II also lists the means of the retracked level IMP derived by the different retrackers over the nine lakes. It can be seen that the IMP of the AMPD algorithm is the largest for all the altimeter data. The larger the IMP value is, the better the performance of the retracking algorithm is when the data are affected by the land noise signal [36]. It should be noted that NPPTR [0.5], NPPTR [0.8], and NPPOR have negative values on Dongping Lake and Taihu Lake, showing that the NPPR algorithm is not suitable for data seriously affected by land. Additionally, SAMOSA has a higher mean standard deviation in many lakes, and its IMP is less than 0 in many lakes, showing that the algorithm is not suitable for processing data with poor waveform quality.

C. Time Series

Table III gives the root-mean-squared errors (RMSEs), calculated by subtracting the difference between the mean of the retracking and *in-situ* water levels time series at the same time,

TABLE III
RMSEs FOR NINE LAKES BETWEEN THE LAKE LEVEL TIME SERIES AND THE *IN-SITU* DATA FROM DIFFERENT ALTIMETER DATA: COMPLETE PERIOD SERIES AND NO-ICE PERIOD SERIES[A]

Datatype	Lake Name	AMPDTR	AMPDOR	MWaPP	NPPTR [0.5]	NPPTR [0.8]	NPPOR	ESA L2	SAMOSA	ALES+
Cryosat-2	Ngoring Lake	0.277 [0.156]	0.283 [0.155]	0.288 [0.156]	0.245 [0.218]	0.233 [0.206]	0.248 [0.218]	0.303 [0.152]		
	Qinghai Lake	0.079 [0.072]	0.071 [0.083]	0.083 [0.079]	0.226 [0.142]	0.165 [0.161]	0.223 [0.151]	0.105 [0.092]		
	Nam Co	0.174 [0.170]	0.177 [0.172]	0.179 [0.178]	0.242 [0.218]	0.229 [0.206]	0.238 [0.213]	0.176 [0.174]		
	Zhari Namco	0.167 [0.184]	0.167 [0.186]	0.169 [0.187]	0.264 [0.217]	0.222 [0.204]	0.255 [0.213]	0.201 [0.235]		
	Bamco	0.114 [0.108]	0.15 [0.150]	0.13 [0.124]	0.143 [0.130]	0.114 [0.107]	0.129 [0.114]	0.159 [0.172]		
	Dagze Co	0.103 [0.115]	0.112 [0.126]	0.12 [0.136]	0.189 [0.157]	0.148 [0.140]	0.182 [0.155]	0.137 [0.151]		
	Dawa Co	0.126 [0.138]	0.126 [0.147]	0.197 [0.230]	0.27 [0.301]	0.239 [0.273]	0.261 [0.293]	0.157 [0.186]		
Sentinel-3	Dongping Lake	0.280 [0.300]	0.295 [0.325]	0.42 [0.472]	0.431 [0.480]	0.427 [0.479]	0.438 [0.486]		0.422 [0.355]	
	Taihu Lake	0.129 [0.129]	0.197 [0.197]	0.128 [0.128]	0.130 [0.130]	0.130 [0.130]	0.131 [0.131]		0.148 [0.148]	
	Qinghai Lake	0.123 [0.053]	0.129 [0.055]	0.164 [0.057]	0.121 [0.053]	0.148 [0.056]	0.122 [0.054]		0.231 [0.071]	
	Nam Co	0.070 [0.051]	0.072 [0.057]	0.059 [0.044]	0.074 [0.057]	0.069 [0.059]	0.073 [0.060]		0.081 [0.062]	
	Zhari Namco	0.141 [0.147]	0.145 [0.147]	0.166 [0.154]	0.142 [0.150]	0.154 [0.147]	0.144 [0.150]		0.183 [0.137]	
	Dagze Co	0.089 [0.083]	0.091 [0.087]	0.075 [0.067]	0.095 [0.087]	0.102 [0.093]	0.086 [0.081]		0.131 [0.114]	
Jason-2	Ngoring Lake	0.331 [0.127]	0.320 [0.195]	0.373 [0.169]	0.35 [0.206]	0.34 [0.134]	0.313 [0.132]			0.341 [0.250]
	Qinghai Lake	0.129 [0.042]	0.174 [0.064]	0.21 [0.071]	0.132 [0.037]	0.174 [0.060]	0.153 [0.047]			0.187 [0.066]
	Zhari Namco	0.101 [0.018]	0.129 [0.023]	0.165 [0.035]	0.119 [0.018]	0.147 [0.029]	0.134 [0.021]			0.144 [0.026]
Jason-3	Zhari Namco	0.161 [0.115]	0.224 [0.169]	0.215 [0.137]	0.140 [0.107]	0.161 [0.104]	0.148 [0.106]			0.138 [0.107]

[a]The RMSEs of no-ice period series are written in square brackets.

for the nine lakes between the lake level time series using different retrackers and the *in-situ* data from different altimeter data. It can be seen that AMPDTR provides excellent results for all the lakes, and the mean RMSEs of lakes, for which Cryosat-2, Sentinel-3, and Jason-2/3 data are available, are 0.149, 0.139, and 0.181 m, respectively. The performances of different retracking algorithms vary for different lakes; thus, the performance of a retracking algorithm should be evaluated for different regions. The Cryosat-2 data are available for seven lakes, and AMPDR has the lowest RMSE for all the lakes except Ngoring Lake and Bamco. In particular for Qinghai Lake, the RMSE from AMPDOR is 0.071 m. The Sentinel-3 data are available for six lakes, and the best results provided by AMPDR are obtained for Dongping Lake (0.280 m) and Zhari Namco (0.141 m). Although no best results are obtained for the other lakes, the results are similar to those from AMPDR. Due to the limitation of Jason-2/3 data quality, the waveforms are easily influenced by the land signal. The results derived by AMPDTR for some lakes are similar compared to those from NPPTR [0.5]. Generally, AMPDTR and AMPDOR give better results than the other retrackers for the four different altimeter data. The water levels for the ice-covered lakes in winter usually have some bias compared with the other seasons [24]. Thus, we also compared different retrackers using data during the warm season only, without ice, in Table III. The ice periods were defined by the regular dates in Section II. For all the retrackers, most of the results in the no-ice period are better than those in the whole period, and the results in both periods derived by AMPDTR and AMPDOR are all excellent. Meanwhile, except for Ngoring Lake, NPPTR [0.5], NPPTR [0.8], and NPPOR achieve

TABLE IV
RMSEs FOR FOUR LAKES BETWEEN THE FUSION LEVEL TIME SERIES AND THE *IN-SITU* DATA

Lake Name	Datatype[a]	AMPDTR	AMPDOR	MWaPP	NPPTR[0.5]	NPPTR[0.8]	NPPOR	CMAN[b]
Qinghai Lake	CSJ2	0.134	0.141	0.177	0.154	0.160	0.156	0.144
Nam Co	CS	0.174	0.178	0.183	0.218	0.207	0.215	0.183
Zhari Namco	CSJ2J3	0.099	0.130	0.135	0.149	0.138	0.146	0.094
Dagze Co	CS	0.090	0.096	0.101	0.198	0.161	0.197	0.102

[a]C stands for Cryosat-2; S stands for Sentinel-3; J3 stands for Jason-3; J2 stands for Jason-2.
[b]The NPPTR[0.5] was used in Sentinel-3**** Jason-3 and Jason-2, while the MWaPP was used in Cryosat-2.

similar results in the no-ice period with AMPDR. Therefore, the proposed AMPDR could improve the results for lakes that ice over in winter to some extent, and can also obtain excellent results in the no-ice period. To evaluate the performance of the AMPDR algorithm in lake level time series from multialtimeter data, multialtimeter lake level time series fusion was obtained for Qinghai Lake, Nam Co, Zhari Namco, and Dagze Co. Table IV lists the RMSEs for the four lakes between the fusion lake level time series using multialtimeter and *in-situ* data. It should be noted that we combined MWaPP and NPPTR [0.5] in processing different altimeter data, NPPTR [0.5] was used for Sentinel-3, Jason-3, and Jason-2, while MWaPP was used for Cryosat-2. Except for Zhari Namco, the fusion lake level time series of the other three lakes extracted by the AMPDTR algorithm were better than those from the other algorithms, indicating that the AMPDR algorithm has excellent performance in monitoring the water level change using multialtimeter data.

The Cryosat-2, Sentinel-3, and Jason-2/3 time series for some lakes and the *in-situ* data are shown in Figs. 8, 9, and 10, respectively. The lake level time series derived by the AMPDTR algorithm agree well with the *in-situ* data. NPPTR[0.5], NPPTR[0.8], and NPPOR could not determine the leading edge of the water reflection for the multipeak waveform, which was often showed in Cryosat-2 data [4], while AMPDTR improves this problem to some extent. AMPDOR performs well for many of the lakes, but its stability is a little worse than that of AMPDTR. Accordingly, we suggest using the AMPDTR algorithm to estimate the lake water level. ESA L2, SAMOSA, and ALES+ are all based on waveform fitting; thus, the performance of the results is largely affected by the quality of waveform data. For example, for Ngoring Lake, the wate-surface signal at many observation points is too weak at the leading edge of the waveform, which leads to the wrong retracking level in some epochs. In fact, the performance of all kinds of retracking algorithms is similar in processing waveforms of good quality. However, the waveforms are often affected by land signal noise, and the performance of the retracking algorithm plays a decisive role in this situation.

In addition, the retracking water level derived by AMPDTR is similar to those from other algorithms when the waveform quality is good, while AMPDTR can also obtain a robust retracking water level for poor waveform quality, showing it to be highly adept at processing complex waveforms. This is of great significance for water level monitoring of small- and medium-sized lakes.

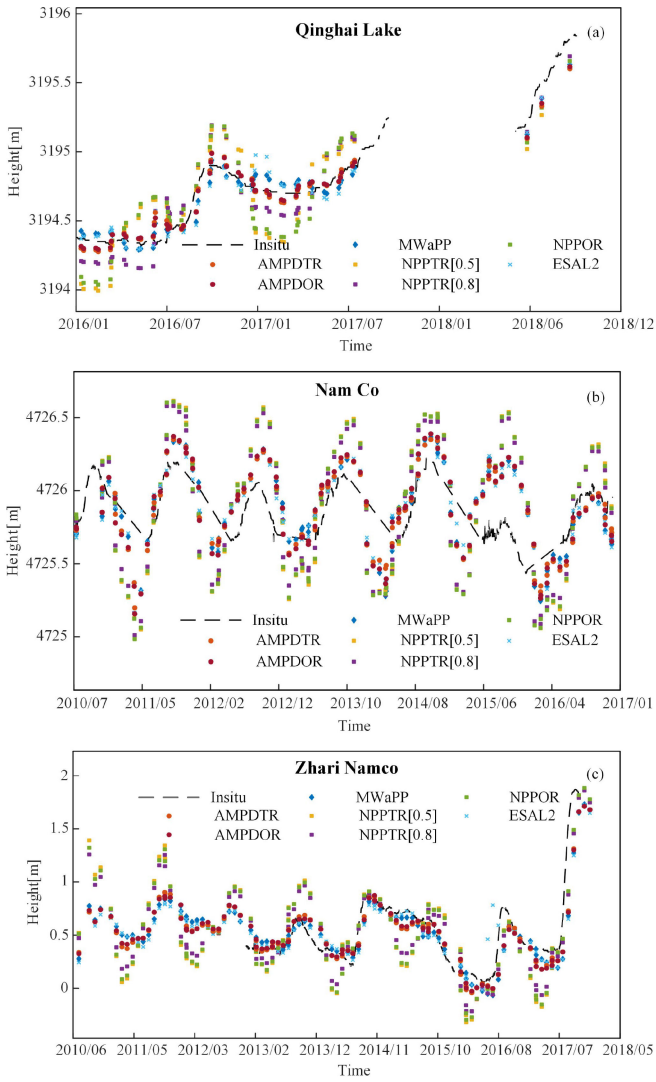

Fig. 8. Cryosat-2 time series for three lakes obtained from different retrackers and compared with the *in-situ* data. (a) Qinghai Lake. (b) Nam Co. (c) Zhari Namco.

V. DISCUSSION

In recent decades, satellite radar altimetry has been successfully used to investigate the water level. Numerous studies have used altimetry observations to extract the water level for inland water bodies such as lakes and rivers [4], [10], [13], [19], [37]–[39]. It is important to extract accurate water levels

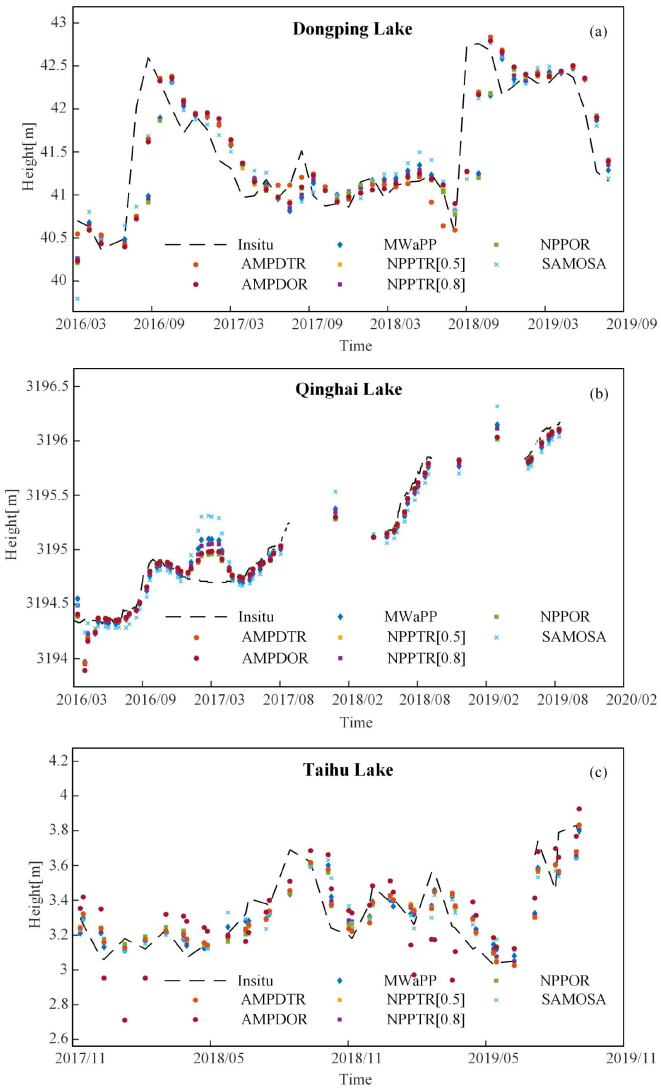

Fig. 9. Sentinel-3 time series for three lakes obtained from different retrackers and compared with the *in-situ* data. (a) Dongping Lake. (b) Qinghai Lake. (c) Taihu Lake.

using a retracking algorithm. Nevertheless, most retrackers are limited to specific altimeter data or to specific regions. The performance of the retracking algorithms varies for different altimeter data, so it is a challenge to select optimal retracking algorithm for monitoring the lake level time series with the fusion of multialtimeter data. Some studies combine retrackers to process waveforms with different characteristics. However, the bias issues that are introduced when combining retrackers mask the potential benefits of combining retrackers [8]. Therefore, we developed an algorithm that is suitable for different altimetry and different situations to derive reliable water levels.

In general, almost all the retracking algorithms mentioned above give good results when the waveform quality is good, but different algorithms display different performances when processing complex waveforms. For instance, MWaPP can avoid noise in the leading edge of a waveform effectively by taking the adjacent waveforms into account, but it may perform incorrectly for some complex waveforms when the waveform is contaminated by multiple surrounding land returns such as vegetation, showing a complex multipeak waveform [4], [40]. NPPR can avoid noise in the trailing edge of waveforms effectively, but it cannot process well or even obtains wrong values when peaks corresponding to water appear late. This is because NPPR retracks the primary peak from the beginning. There is no doubt that the SAMOSA3 retracker provides very stable water levels. The benefit of using the SAMOSA3 retracker is, however, concealed in regions like inland water, as it cannot obtain the water level of the multipeak waveform, and the computation is time consuming. The AMPDR retracking algorithm obtains similar results to the other algorithms when the waveform quality is good, and it can also solve the problem of complex waveforms mentioned above to a certain extent. Although not all waveform data can be processed best by AMPDR, it can be highly adept to the complex changes of waveform data and can handle more observations effectively without reducing the precision, which is of great significance to monitoring the lake levels of small- and medium-sized lakes. It should be noted that AMPDR performs excellently in most lakes, such as Qinghai Lake and Nam Co. For Qinghai Lake, the RMSE of 0.071 m from AMPDOR is better than the RMSE of 0.085 m given by [4]. For Nam Co, the RMSE of 0.174 m from AMPDTR is better than the RMSE of 0.180 m given by [41]. Most of the existing retracking algorithms are all based on a certain type of altimetry; thus, the MWaPP algorithm was proposed to process the Cryosat-2 SAR mode data, but should be easily applicable to any SAR data. This has been confirmed by Jiang *et al.* [19] with only a few simple adjustments of MWaPP for Sentinel-3. Although it can be used for Jason-2/3, its accuracy is not as good as that of the NPPTR algorithm. Compared with other algorithms, AMPDR is not a pure processing method for a certain altimeter waveform, and its core function is to obtain a threshold level (DistanceThres) to identify the water-surface signal of the waveform using a robust statistical method, so it cannot be affected by the type of altimeter data. This is important to monitor long time series of the lake level by fusing multialtimeter data. Moreover, the data quality and availability are also of great significance to monitor lake level time series. As for Sentinel-3, the Open-Loop Tracking Command version 5 (OLTC V5) has significantly improved the placement of the range window, and more effective observation could be obtained compared to the data over some mountain rivers prior to OLTC V5 (March 2019) [42], [43]. It may be easier to monitor the water levels of small- and medium-sized lakes with the help of OLTC V5, but it also poses some new challenges: steep changes in the receiving window position can have detrimental effects on the water level [42]. Due to the utilization of a robust statistical method, AMPDR may solve this problem to some extent.

According to the results given in this study, the AMPDR algorithm can provide the stable water level. However, it cannot provide good results in some cases, when all the waveforms along the track are heavily contaminated, which would lead to a wrong retracking level. This situation may occur when the lake area is small or the track is distributed along the shore

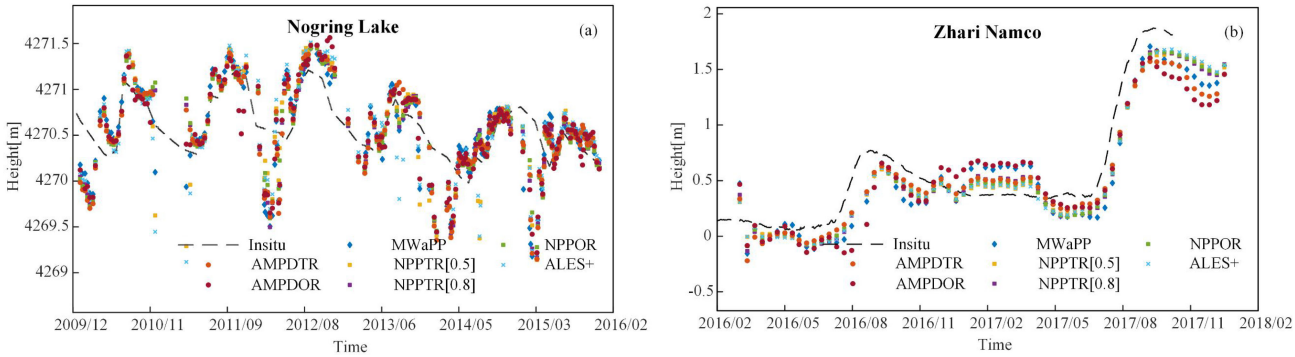

Fig. 10. Jason-2/3 time series for two lakes obtained from different retrackers and compared with the *in-situ* data. (a) Nogring Lake. (b) Zhari Namco.

of the lake with complex surrounding terrain. For example, for Ngoring Lake crossed by Cryosat-2 and Jason-2, AMPDR shows poor performance. This is because, in Ngoring Lake, there are lots of complex waveforms with weak surface reflected signals, which may be the result of the environment in Ngoring Lake, and signals from the altimeter for dense vegetation are very different from those directly from the water body [43]. Additionally, the moving average window of the AMPDR algorithm in this article is 11 gates, indicating that the algorithm can only detect the peak when the interval between two successive peaks is more than five gates. Therefore, if there is a situation when the interval between two successive peaks is less than five gates, it may affect the calculation of the shortest path of the "point-cloud" and decrease the precision of the algorithm. The high RMSE of the water level in Dongping Lake crossed by Sentinel-3 may be not because of the algorithm itself. Dongping Lake is a large reservoir where the water levels are controlled by a management agency, its track level is stable, and the waveforms show good quality. But it demonstrates a high RMSE, which may be caused by the difference of five hours between the *in-situ* level and the estimated level. The large deviation of the water level may be caused by the discharge of water into the Yellow River on that day.

The number of altimetry observation points is usually small in small- and medium-sized lakes and narrow rivers, and the data are more susceptible to being contaminated by land signals. The AMPDR retracking algorithm proposed in this article can derive more stable and reliable height information from the limited observation data. The algorithm can also be applied to other altimeters, such as Envisat, TOPEX/Poseidon, and possibly to the upcoming Jason-CS mission, which will further improve the ability of monitoring the water level of inland surfaces with complex surrounding terrain. In addition, high-precision water levels can be combined with other prior information and hydrological modeling to analyze the hydrologic information of global basins with no data or insufficient data, which will be further discussed in the future.

VI. Conclusion

In this study, a novel retracker (AMPDR) was proposed that can be applied to various altimeter data. AMPDR is not a pure, single-waveform retracker, and its key is to identify the water-surface signal of the waveform by using peak detection and a robust statistical method, which can process the complex waveforms contaminated by land signals. We evaluated the retracking performance of eight different algorithms for Cryosat-2 SARin, Sentinel-3, and Jason-2/3 waveforms in comparison to the *in-situ* data of nine Chinese lakes with different characteristics. The eight algorithms used in this study were AMPDR, MWaPP, NPPTR [0.5], NPPTR [0.8], NPPOR, ESA L2, SAMOSA, and ALES+.

The results showed that AMPDR outperformed the other retrackers in processing different altimeter data. It can handle more observations effectively without reducing the precision, which is of great significance in monitoring the lake levels of small- and medium-sized lakes. Although AMPDR algorithm cannot handle in all kinds of waveform data optimally, it can adapt to many kinds of complex waveform and extract reliable height information from complex waveforms contaminated by land signals. However, having an interval between two successive peaks of less than five gates may result in an incorrect retracking height, which may occur when there is severe contamination by land signals. Additionally, considering the influence of system bias caused by the combination of retrackers, we suggest using the AMPDTR algorithm in multialtimeter data for lake level monitoring, which can be used to obtain more stable time series of lake levels.

To further improve precision and RMSEs, we also suggest using more robust methods to detect and determine the outliers in the lake level time series. Finally, the retrackers presented here are only used to monitor the big lakes using Cryosat-2, Sentinel-3, and Jason-2/3 data, but they should also be easily applicable to the other altimeter data. Moreover, the AMPDR may also have the potential to monitor the water levels of small- and medium-sized lakes or some rivers.

Acknowledgment

The authors would like to thank the European Space Agency and Centre National d'Etudes Spatiales for providing the altimeter data, and the Bureau of Hydrology and Water Resources of Qinghai Province, the Yellow River Commission of the

Ministry of Water Resources, the Department of Water Resources of JiangSu Province, and the Institute of Tibetan Plateau Research, Chinese Academy of Sciences for providing *in-situ* gauge measurements of water levels. They would also like to thank the anonymous reviewers for their voluntary work and the constructive comments which helped to improve this article.

REFERENCES

[1] C. M. Birkett, "Contribution of the TOPEX NASA radar altimeter to the global monitoring of large rivers and wetlands (B)," *Water Resour. Res.*, vol. 34, no. 5, pp. 1223–1239, 1998.

[2] J. Liao, L. Gao, and X. Wang, "Numerical simulation and forecasting of water level for Qinghai lake using multi-altimeter data between 2002 and 2012," *IEEE J. Sel. Topics Appl. Earth Observ. Remote Sens.*, vol. 7, no. 2, pp. 609–622, Feb. 2014.

[3] J. F. Crétaux *et al.*, "Lake volume monitoring from space," *Surv. Geophys.*, vol. 37, no. 2, pp. 269–305, 2016.

[4] H. Xue, J. Liao, and L. Zhao, "A modified empirical retracker for lake level estimation using Cryosat-2 SARin data," *Water (Switzerland)*, vol. 10, no. 11, 2018, Art. no. 1584.

[5] X. Li, D. Long, Q. Huang, P. Han, F. Zhao, and Y. Wada, "High-temporal-resolution water level and storage change data sets for lakes on the Tibetan plateau during 2000–2017 using multiple altimetric missions and Landsat-derived lake shoreline positions," *Earth Syst. Sci. Data*, vol. 11, no. 4, pp. 1603–1627, 2019.

[6] P. H. Gleick, "Global freshwater resources: Soft-path solutions for the 21st century," *Science*, vol. 302, no. 5650, pp. 1524–1528, 2003.

[7] S. Shu *et al.*, "Analysis of Sentinel-3 SAR altimetry waveform retracking algorithms for deriving temporally consistent water levels over ice-covered lakes," *Remote Sens. Environ.*, vol. 239, no. December 2019, 2020, Art. no. 111643.

[8] H. Villadsen, X. Deng, O. B. Andersen, L. Stenseng, K. Nielsen, and P. Knudsen, "Improved inland water levels from SAR altimetry using novel empirical and physical retrackers," *J. Hydrol.*, vol. 537, pp. 234–247, 2016.

[9] C. Hwang *et al.*, "Lake level changes in the Tibetan plateau from Cryosat-2, SARAL, ICESat, and Jason-2 altimeters," *Terrestrial Atmos. Ocean. Sci.*, vol. 30, no. 1, pp. 1–18, 2019.

[10] A. Z. Zaidi *et al.*, "Indus river water level monitoring using satellite radar altimetry," *Adv. Space Res.*, to be published, doi: 10.1016/j.asr.2020.03.044.

[11] S. Bogning *et al.*, "Monitoring water levels and discharges using radar altimetry in an ungauged river basin: The case of the Ogooué," *Remote Sens.*, vol. 10, no. 2, 2018, Art. no. 350.

[12] T. Yuan *et al.*, "Absolute water storages in the Congo river floodplains from integration of InSAR and satellite radar altimetry," *Remote Sens. Environ.*, vol. 201, no. September, pp. 57–72, 2017.

[13] D. Kim *et al.*, "Ensemble learning regression for estimating river discharges using satellite altimetry data: Central Congo river as a test-bed," *Remote Sens. Environ*, vol. 221, no. November 2018, pp. 741–755, 2019.

[14] C. M. Emery *et al.*, "Assimilation of wide-swath altimetry water elevation anomalies to correct large-scale river routing model parameters," *Hydrol. Earth Syst. Sci.*, vol. 24, no. 5, pp. 2207–2233, 2020.

[15] C. Kittel, K. Nielsen, C. Tøttrup, and P. Bauer-Gottwein, "Informing a hydrological model of the Ogooué with multi-mission remote sensing data," *Hydrol. Earth Syst. Sci.*, vol. 22, no. 2, pp. 1453–1472, 2018.

[16] E. Park, "Characterizing channel-floodplain connectivity using satellite altimetry: Mechanism, hydrogeomorphic control, and sediment budget," *Remote Sens. Environ.*, vol. 243, no. March, 2020, Art. no. 111783.

[17] G. Liu, F. W. Schwartz, K.-H. Tseng, and C. K. Shum, "Discharge and water-depth estimates for ungauged rivers: Combining hydrologic, hydraulic, and inverse modeling with stage and water-area measurements from satellites," *Water Resour. Res.*, vol. 51, pp. 6017–6035, 2015.

[18] J. Dumont *et al.*, "Jason-3 product handbook," Accessed: Jun. 6, 2019. [Online]. Available: https://www.nodc.noaa.gov/media/pdf/ jason2/j3_user_handbook.pdf

[19] L. Jiang, K. Nielsen, S. Dinardo, O. B. Andersen, and P. Bauer-Gottwein, "Evaluation of Sentinel-3 SRAL SAR altimetry over Chinese rivers," *Remote Sens. Environ.*, vol. 237, no. August 2019, 2020, Art. no. 111546.

[20] C. Bouzinac, "CryoSat-2 product handbook," Accessed: Jan. 1, 2018. [Online]. Available: https://earth.esa.int/documents/10174/125272/CryoSat_Product_Handbook

[21] M. Jain, O. B. Andersen, J. Dall, and L. Stenseng, "Sea surface height determination in the arctic using Cryosat-2 SAR data from primary peak empirical retrackers," *Adv. Space Res.*, vol. 55, no. 1, pp. 40–50, 2015.

[22] Q. Huang *et al.*, "An improved approach to monitoring Brahmaputra river water levels using retracked altimetry data," *Remote Sens. Environ.*, vol. 211, no. July 2017, pp. 112–128, 2018.

[23] C. Yuan, P. Gong, H. Zhang, H. Guo, and B. Pan, "Monitoring water level changes from retracked Jason-2 altimetry data: A case study in the Yangtze river, China," *Remote Sens. Lett.*, vol. 8, no. 5, pp. 399–408, 2017.

[24] S. Shu *et al.*, "Analysis of Sentinel-3 SAR altimetry waveform retracking algorithms for deriving temporally consistent water levels over ice-covered lakes," *Remote Sens. Environ.*, vol. 239, no. December 2019, 2020, Art. no. 111643.

[25] D. Ganguly, S. Chander, S. Desai, and P. Chauhan, "A subwaveform-based retracker for multipeak waveforms: A case study over UKAI dam/reservoir," *Marine Geodesy*, vol. 38, no. March, pp. 581–596, 2015.

[26] J. Chen and J. Liao, "Monitoring lake level changes in China using multi-altimeter data (2016–2019)," *J. Hydrol.*, vol. 590, no. April, 2020, Art. no. 125544.

[27] N. K. Pavlis, S. A. Holmes, S. C. Kenyon, and J. K. Factor, "The development and evaluation of the earth gravitational model 2008 (EGM2008)," *J. Geophys. Res. Solid Earth*, vol. 117, no. 4, pp. 1–38, 2012.

[28] K. Nielsen, L. Stenseng, O. B. Andersen, H. Villadsen, and P. Knudsen, "Validation of Cryosat-2 SAR mode based lake levels," *Remote Sens. Environ.*, vol. 171, pp. 162–170, 2015.

[29] F. Scholkmann, J. Boss, and M. Wolf, "An efficient algorithm for automatic peak detection in noisy periodic and quasi-periodic signals," *Algorithms*, vol. 5, no. 4. pp. 588–603, 2012.

[30] D. J. Wingham, C. G. Rapley, and H. Griffiths, "New techniques in satellite altimeter tracking systems," in *Proc. Dig.—Int. Geosci. Remote Sens. Symp.*, 1986, pp. 1339–1344.

[31] E. W. Dijkstra, "A note on two problems in connexion with graphs," *Numerische Mathematik*, vol. 1, pp. 269–271, 1959.

[32] D. J. Wingham *et al.*, "CryoSat: A mission to determine the fluctuations in earth's land and marine ice fields," *Adv. Sp. Res.*, vol. 37, no. 4, pp. 841–871, 2006.

[33] C. Ray *et al.*, "SAR altimeter backscattered waveform model," *IEEE Trans. Geosci. Remote Sens.*, vol. 53, no. 2, pp. 911–919, Feb. 2015.

[34] M. Passaro *et al.*, "ALES+: Adapting a homogenous ocean retracker for satellite altimetry to sea ice leads, coastal and inland waters," *Remote Sens. Environ.*, vol. 211, no. July 2017, pp. 456–471, 2018.

[35] L. Jiang, O. B. Andersen, K. Nielsen, G. Zhang, and P. Bauer-Gottwein, "Influence of local geoid variation on water surface elevation estimates derived from multi-mission altimetry for lake Namco," *Remote Sens. Environ.*, vol. 221, no. November 2018, pp. 65–79, 2019.

[36] C. Hwang, J. Guo, X. Deng, H. Y. Hsu, and Y. Liu, "Coastal gravity anomalies from retracked Geosat/GM altimetry: Improvement, limitation and the role of airborne gravity data," *J. Geodesy*, vol. 80, no. 4, pp. 204–216, 2006.

[37] S. Coss *et al.*, "Global river radar altimetry time series (GRRATS): New river elevation earth science data records for the hydrologic community," *Earth Syst. Sci. Data*, vol. 12, no. 1, pp. 137–150, 2020.

[38] Q. Gao *et al.*, "Analysis of retrackers' performances and water level retrieval over the Ebro river basin using Sentinel-3," *Remote Sens.*, vol. 11, no. 6, pp. 1–25, 2019.

[39] X. Deng, W. E. Featherstone, C. Hwang, and P. A. M. Berry, "Estimation of contamination of ERS-2 and POSEIDON satellite radar altimetry close to the coasts of Australia," *Marine Geodesy*, vol. 25, no. 4, pp. 249–271, 2002.

[40] P. Li, H. Li, F. Chen, and X. Cai, "Monitoring long-term lake level variations in middle and lower Yangtze basin over 2002–2017 through integration of multiple satellite altimetry datasets," *Remote Sens.*, vol. 12, no. 9, 2020, Art. no. 1448.

[41] C. Song, Q. Ye, and X. Cheng, "Shifts in water-level variation of namco in the central Tibetan plateau from ICESat and Cryosat-2 altimetry and station observations," *Sci. Bull.*, vol. 60, no. 14, pp. 1287–1297, 2015.

[42] C. Kittel, L. Jiang, C. Tøttrup, and P. Bauer-Gottwein, "Sentinel-3 radar altimetry for river monitoring—A catchment-scale evaluation of satellite water surface elevation from Sentinel-3A and Sentinel-3B," *Hydrol. Earth Syst. Sci. Discuss.*, no. May, pp. 1–35, 2020.

[43] P. Maillard, N. Bercher, and S. Calmant, "New processing approaches on the retrieval of water levels in envisat and SARAL radar altimetry over rivers: A case study of the São Francisco river, Brazil," *Remote Sens. Environ.*, vol. 156. pp. 226–241, 2015.

Jiaming Chen received the B.S. degrees in remote sensing science and technology from Wuhan University, Wuhan, China, in 2018. He is currently working toward the M.S. degree in cartography and geography information system with the Key Laboratory of Digital Earth Science, Aerospace Information Research Institute, Chinese Academy of Sciences, Beijing, China.

His research focuses on the altimetry data for land applications, especially on the lakes and rivers.

Jingjuan Liao received the B.S. and M.S. degrees in geosciences from Nanjing University, Nanjing, China, in 1987 and 1990, respectively, and the Ph.D. degree in geophysics from the Institute of Geophysics, Chinese Academy of Sciences, Bejing, China, in 1993.

Since 1993, she has been working on radar remote sensing applications as a Researcher with the Institute of Remote Sensing Applications, Chinese Academy of Sciences. She has rendered the institute great service in several research projects. Since 2007, she has been working on microwave remote-sensing application as a Professor with the Center for Earth Observation and Digital Earth and the Institute of Remote Sensing and Digital Earth, Chinese Academy of Sciences. She is currently working with the Key Laboratory of Digital Earth Science, Aerospace Information Research Institute, Chinese Academy of Sciences. She has completed several research projects, and authored and coauthored more than 100 paper in relevant journals. Her current research interests include microwave scattering model, data processing, and surface parameters estimation.

Chao Wang received the B.S. degrees in electronic engineering from Zhengzhou University, Zhengzhou, China, in 1996, and the M.S. degree in geomatics engineering from the Henan University of Technology, Zhengzhou, China, in 2006.

He is currently with the Institute of Geography, Henan Academy of Sciences, Zhengzhou, China as a Senior Engineer. He has rendered several research projects and authored and coauthored 18 papers and took six patents. His research interests focus on multisource remote sensing data acquisition and land resources survey.